Bulletin of the Seismological Society of America, Vol. 98, No. 2, pp. 620–635, April 2008, doi: 10.1785/0120060185

# Testing Small-Aperture Array Analysis on Well-Located Earthquakes, and Application to the Location of Deep Tremor

by Mario La Rocca, Danilo Galluzzo, Steve Malone, Wendy McCausland,* Gilberto Saccorotti,† and Edoardo Del Pezzo

Abstract We have here analyzed local and regional earthquakes using array techniques with the double aim of quantifying the errors associated with the estimation of propagation parameters of seismic signals and testing the suitability of a probabilistic location method for the analysis of nonimpulsive signals. We have applied the zero-lag cross-correlation method to earthquakes recorded by three dense arrays in Puget Sound and Vancouver Island to estimate the slowness and back azimuth of direct *P* waves and *S* waves. The results are compared with the slowness and back azimuth computed from the source location obtained by the analysis of data recorded by the Pacific Northwest seismic network (PNSN). This comparison has allowed a quantification of the errors associated with the estimation of slowness and back azimuth obtained through the analysis of array data. The statistical analysis gives $\sigma_{BP} = 10°$ and $\sigma_{BS} = 8°$ as standard deviations for the back azimuth and $\sigma_{SP} = 0.021$ sec/km and $\sigma_{SS} = 0.033$ sec/km for the slowness results of the *P* and *S* phases, respectively. These values are consistent with the theoretical relationship between slowness and back azimuth and their uncertainties.

We have tested a probabilistic source location method on the local earthquakes based on the use of the slowness estimated for two or three arrays without taking into account travel-time information. Then we applied the probabilistic method to the deep, nonvolcanic tremor recorded by the arrays during July 2004. The results of the tremor location using the probabilistic method are in good agreement with those obtained by other techniques. The wide depth range, of between 10 and 70 km, and the source migration with time are evident in our results. The method is useful for locating the source of signals characterized by the absence of pickable seismic phases.

## Introduction

Seismic arrays have been used in seismology for several decades to investigate the hidden features of seismic waves. They are particularly useful for those waves characterized by emergent onset, in situations where a sparse seismic network cannot be deployed around the source, and for cases where signal-to-noise ratio improvements are needed. Exotic seismic signals, such as volcanic tremors, low-frequency earthquakes, coda waves, seismic noise, and chemical and nuclear explosions are the typical subjects for array analysis. Because the variety of sources is so wide, several techniques have been developed in both the time and frequency domains, and they have been tested to yield the most useful information from a given dataset.

Traditional methods of determining earthquake hypocenters are based on the minimization of travel-time residuals of phases picked at network seismic stations. These methods are computationally fast and give good results for events that are characterized by sharp phases recorded by a well-distributed set of stations. However, they are not well suited for events that are characterized by emergent onset or by the absence of sharp pulses. Therefore, they cannot work for continuous sources such as tremors.

As part of an array study carried out during the summer of 2004 to record and analyze deep tremors associated with episodic slip, we recorded a range of regular local and regional tectonic earthquakes. In the present study, we use the locations of these earthquakes, as determined by conventional techniques of picking phase arrivals at regional

*Present address: Cascade Volcano Observatory, U.S. Geological Survey, 1300 Southeast Cardinal Street, Building 10, Suite 100, Vancouver, Washington, 98683-9589; wmccausland@usgs.gov.

†Present address: Istituto Nazionale di Geofisica e Vulcanologia, Sezione di Pisa, Via U. della Faggiola, 32, 56126 Pisa, Italy; saccorotti@pi.ingv.it.

network stations, to study the accuracy of locations determined by array analysis techniques. For this comparison, we have selected a set of earthquakes that occurred in the same region as the deep tremor.

For array analysis, the frequency–wavenumber spectral method was an early development (Capon, 1969), and it was later refined in the multiple-source separation technique (Schmidt, 1986; Goldstein and Archuleta, 1987, 1991). Other techniques based on the estimation of the wave-field coherence in the time domain are more appropriate for detailed analysis of short transient signals (Frankel *et al.*, 1991; Del Pezzo *et al.*, 1997).

A problem that still partially remains to be resolved in array analysis is the determination of the uncertainty associated with the estimate of the slowness (or wavenumber) vector components. The errors depend on many factors, such as the array configuration, the extension and number of stations, the signal-to-noise ratio, the coherence of the seismic signal among the stations, the coherence of the seismic noise, and the site effects. Other factors that contribute to the uncertainty, such as sampling rates and the density of grid searches, can usually be made small enough so as to be negligible. While theoretical and empirical methods have been proposed and applied in many studies, a general method that is applicable to any array and any kind of signal is not available. Saccorotti and Del Pezzo (2000) and references therein discussed in detail the theoretical errors that are associated with the wave-vector components estimated by array methods in the time domain. In the present study, we compare such theoretical error estimates to experimental results. We use here zero-lag cross-correlation (ZLCC) analysis for estimating back azimuth and slowness of the main phases of well-located earthquakes, and we compare these values with those determined by the ordinary hypocenter locations based on a dense, regional network. We also use the array analysis of earthquake phases, combined with a probabilistic source location procedure, to determine how the array analysis error estimates propagate into the source location problem.

We have used the data recorded by three short-period seismic arrays deployed in the Puget Sound area during the summer of 2004 to record the anticipated episodic tremor and slip (ETS) event that occurred in July 2004 (La Rocca *et al.*, 2005). The arrays were located on Lopez Island (Lopez array, six stations), North Olympic Peninsula (Sequim array, seven stations) and Vancouver Island (Sooke array, six sta-

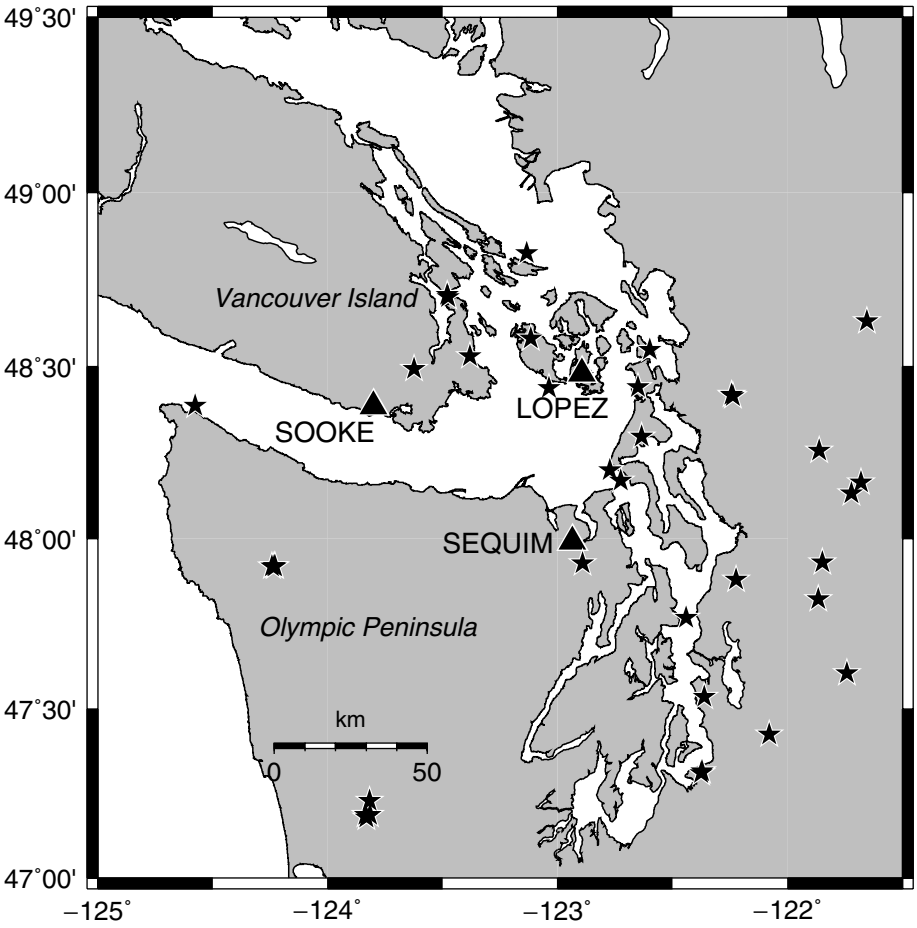


**Figure 1.** Map of the northern Washington and British Columbia region. The three-array sites are indicated by triangles. Stars show the epicenters of the closest earthquakes analyzed in this study. The array configurations are shown in Figure 4.

tions), as shown in Figure 1. Hundreds of local and regional earthquakes were recorded between early April and late July. Those that were well recorded by at least five stations of the same array have been analyzed in detail using the ZLCC method. The comparison of estimated slowness and back azimuth with the values computed from the well-located sources, along with some considerations of the theoretical array response, allows estimation of the array resolution capability. The probabilistic source location method used by La Rocca *et al.* (2004) to locate the source of low-frequency explosion quakes for Stromboli volcano was applied to some of the local earthquakes to test the effectiveness of this method. While this error-testing investigation is important in its own right, it is critical for subsequent array analysis of deep tremor signals, and particularly for those recorded by the same arrays. Several tremor signals recorded by the arrays were located using the same probabilistic method.

Throughout the present study, we refer to the location based on the phase picking at the regional Pacific Northwest seismic network (PNSN) network as the network location and the location based on the results of array analysis as the array location. The frequently used symbols are $S$ for slowness, $\Delta S$ for slowness difference, $V$ for apparent velocity (defined as $V = 1/S$), $\varphi$ for back azimuth (the direction from the station to the epicenter), and $\Delta\varphi$ for back-azimuth difference. $\sigma_S$ and $\sigma_B$ will indicate the standard deviations of the slowness and back-azimuth distributions, while the subscripts $P$ and $S$ are used for $P$ waves and $S$ waves, respectively.

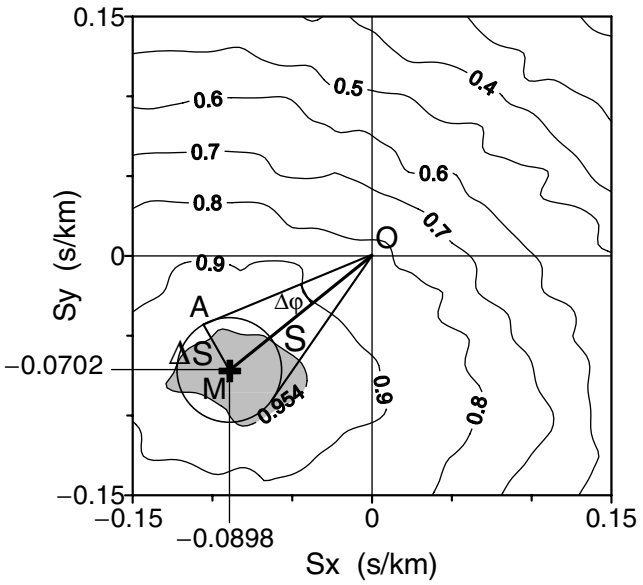


**Figure 2.** Slowness spectrum obtained by analysis of the $P$ waves of earthquake 200405131943 at the Lopez array. The maximum of this spectra (indicated with a cross) reaches 0.974. Its coordinates define the slowness vector estimated by the ZLCC analysis of this seismic phase, here represented by the O–M line. The corresponding apparent velocity is 8.75 km/sec, and the back azimuth is 232°. The circle of radius $\Delta S$ used to define the uncertainty of these estimated values corresponds roughly to a correlation level of 0.954, as indicated by the shaded area; therefore $\Delta C = 0.02$. The error on the back azimuth, $\Delta\varphi$, is the angle subtended by A–M at point O.

## Array Analysis Method and Array Response

The ZLCC array method (Frankel *et al.*, 1991; Del Pezzo *et al.*, 1997; Saccorotti and Del Pezzo, 2000) searches for the absolute maximum of a correlation function computed over a regular square grid in slowness space. For each node of the grid, the correlation is computed as the mean of the normalized correlation pairs $C_{ij}$:

$$c_{ij} = \frac{\sum_{k=1}^{M} A_k^i A_k^j}{\sqrt{\sum_{k=1}^{M} (A_k^i)^2 \sum_{k=1}^{M} (A_k^j)^2}}, \tag{1}$$

where $A_k^i$ is the $k$th sample of the seismogram recorded at the $i$th station.

The grid step taken is small enough to make the uncertainty of the slowness corresponding to the correlation maximum negligible. For an array composed of many stations arranged in an optimal configuration such that the array response is independent of the propagation direction, the uncertainties associated with the two components of the slowness vector are the same. Under these assumptions, we define a circle of radius $\Delta S = \Delta S_x = \Delta S_y$ in the grid search around the maximum $C_{\max}$, for which the correlation values are within $\Delta C$ of $C_{\max}$, as shown in Figure 2. From Figure 2, the following relationships between $\Delta S$ and the back-azimuth uncertainty $\Delta\varphi$ are obtained:

$$\Delta\varphi = \arcsin(\Delta S/S), \tag{2}$$

$$\Delta\varphi = \arcsin(\Delta S V). \tag{3}$$

The error, $\Delta V$, on the apparent velocity $V$ is computed as

$$\Delta V = \frac{1}{2}(V_{\max} - V_{\min}) = \frac{1}{2}\left(\frac{1}{S - \Delta S} - \frac{1}{S + \Delta S}\right) = \frac{\Delta S}{S^2 - \Delta S^2} = \frac{V^2 \Delta S}{1 - V^2 \Delta S^2}. \tag{4}$$

These functions are plotted in Figure 3 for several values of $\Delta S$. As expected, the uncertainties of the apparent velocity and back azimuth have an exponential trend as the apparent velocity increases. In the case of a seismic phase propagating with a slowness smaller than $\Delta S$, only a lower limit for the apparent velocity can be estimated, while the back azimuth cannot be determined.

The response of an $N$-station array, $B(S)$, is computed through the formula (Capon, 1969):

$$B(S) = \frac{1}{N^2}\left|\sum_{j=1}^{N} \exp(i\omega \mathbf{S} \cdot \mathbf{r}_j)\right|^2, \tag{5}$$

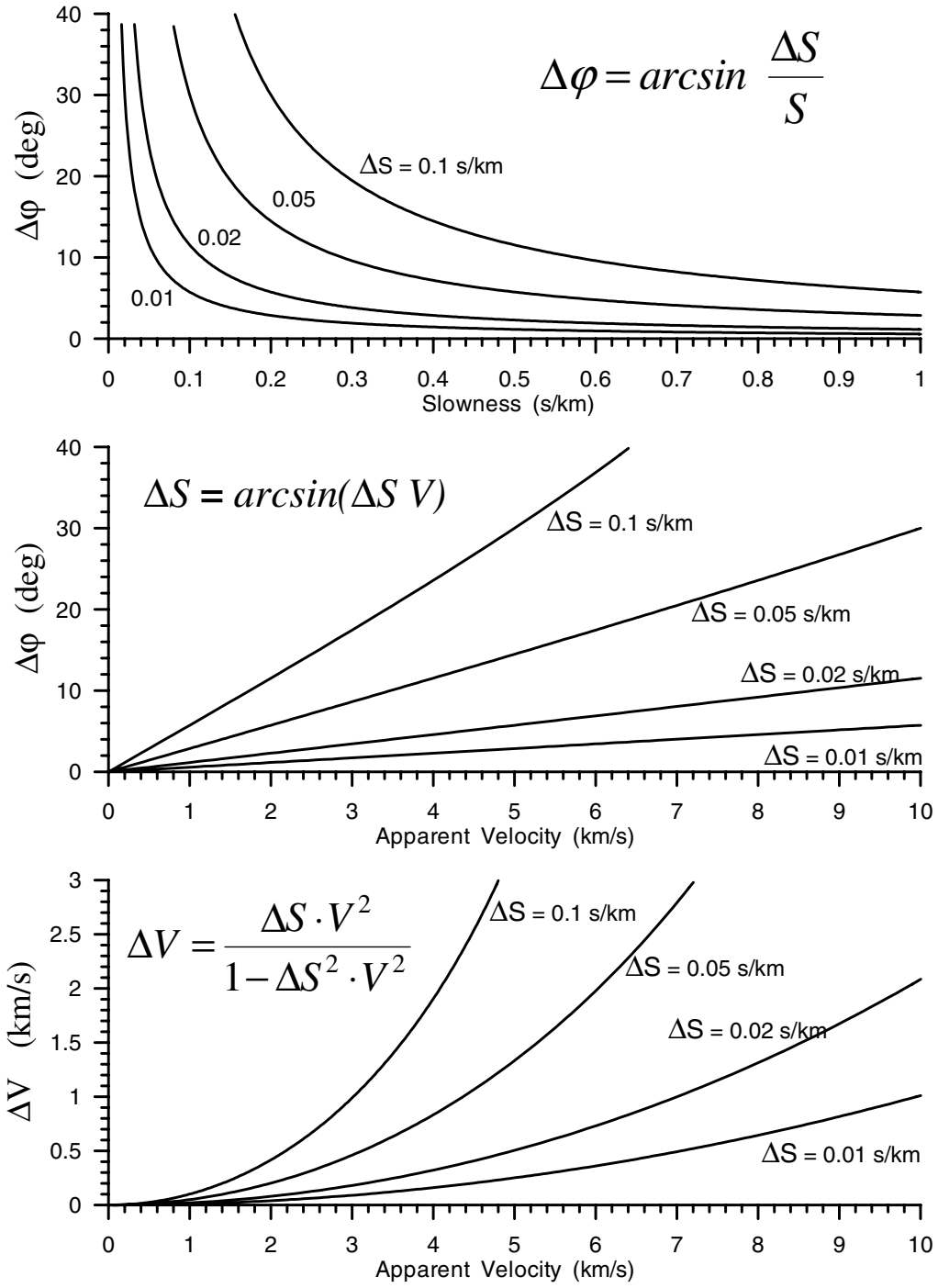


**Figure 3.** Families of curves for different values of the uncertainty $\Delta S$. The errors on back azimuth and apparent velocity as functions of apparent velocity and slowness are shown.

where $\mathbf{r}_j$ is the position of the $j$th station. Figure 4 shows the array response computed for the three arrays for two different values of $\omega$. The shapes of the isolines are very close to a circle for the Lopez and Sequim arrays, indicating that the array analysis results are independent of the propagation direction. At the Sooke array, the elliptical shape reflects the elongated array configuration and indicates a slightly anisotropic response. At higher frequencies, the peak of the correlation function is much sharper than that at low frequencies. This implies that high frequency seismic signals should be resolved much more accurately than low-frequency signals. Unfortunately, the coherence of the seismic wave field usually decreases as the frequency increases, and this usually compensates for the sharpening of the ideal response peak.

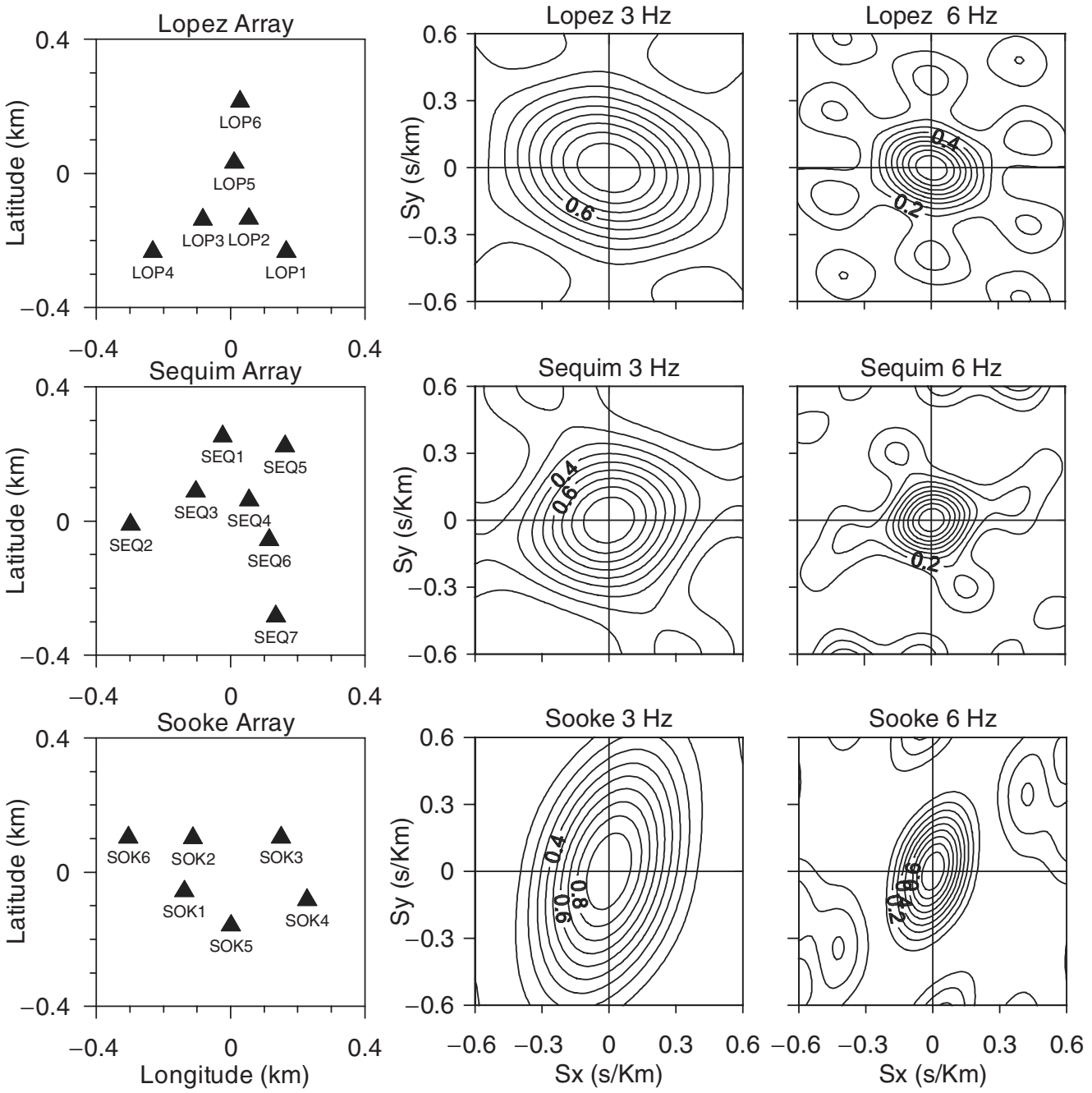


**Figure 4.** The three-array configurations (left column) and their ideal response at two different frequencies (central column, 3 Hz; right column, 6 Hz).

## Data Analysis

The dataset used for the present study consisted of 51 earthquakes, 19 of which were located at distances greater than 100 km from each array, and hence were classified as regional events. The 32 local or near-regional epicenters are shown in Figure 1. The distances of the events ranged from 8 to 658 km, whereas the source depth was between 0 and 30 km. The magnitudes were in the range of 0.8–6.4. We have only analyzed the earthquakes that were recorded by at least five stations of the same array. At the Sooke array, we also required stations SOK3 and SOK5 to be among this minimum number of five stations to ensure a satisfactory array configuration. These conditions were satisfied by 48 events for the Lopez array, 45 for Sequim, and 24 for Sooke.

Most of the data were analyzed in one or two of the frequency bands of 2–4, 3–6, or 4–8 Hz. The ZLCC analysis was applied to a sliding window of length in the range of 0.5–2 sec, depending on the frequency band. For events with a source azimuth far from the north–south and east–west directions, the horizontal components were rotated to radial

and transverse based on the back azimuth obtained by the analysis of the vertical component alone. As an example, Figure 5 shows the results of the array analysis for earthquake 200405131943 at the Sequim array. For some events in the range of 80–180 km, an apparent *PmP* phase is recognizable in the seismograms. For events farther than about 250 km, two different *P* phases are sometimes seen. In other cases, the low signal-to-noise ratio and/or the nodal position of the array with respect to the focal mechanisms do not allow for a reliable solution of the direct *P* and *S* phases. Therefore, the number of seismic phases for which the results of array analysis can be compared with the expected values is different from the number of events analyzed. We estimated apparent velocity and back azimuth for 52 *P* and 58 *S* phases at the Lopez array, 50 *P* and 45 *S* phases at Sequim, and 24 *P* and 20 *S* phases at Sooke, respectively.

Because the *S*-wave onset is superimposed on the *P*-wave coda, the *S*-wave signal-to-noise ratio is generally lower than that of the *P* wave. Moreover, the presence of conversion of *SV* to *P* just before the direct *S* wave may further reduce the quality of the direct shear-wave signal. However, these unfavorable conditions are partly compensated for by the lower frequency and lower apparent velocity of the *S* waves. This compensation arises because the coherence of the wave field among the stations is usually higher at lower frequencies and because the error of the apparent velocity and back azimuth decreases with decreasing apparent velocity, as stated by formulas (2) and (3).

Hereinafter, given the array positions and a velocity model, we will refer to the slowness and back azimuth computed from the network determined location as the expected slowness and the expected back azimuth. For the selected dataset, we estimated the expected back azimuth and slowness for each earthquake at each array. The slowness was computed using the TauP software (Crotwell *et al.*, 1999) with the standard PNSN, P3-layered velocity model (Cross-

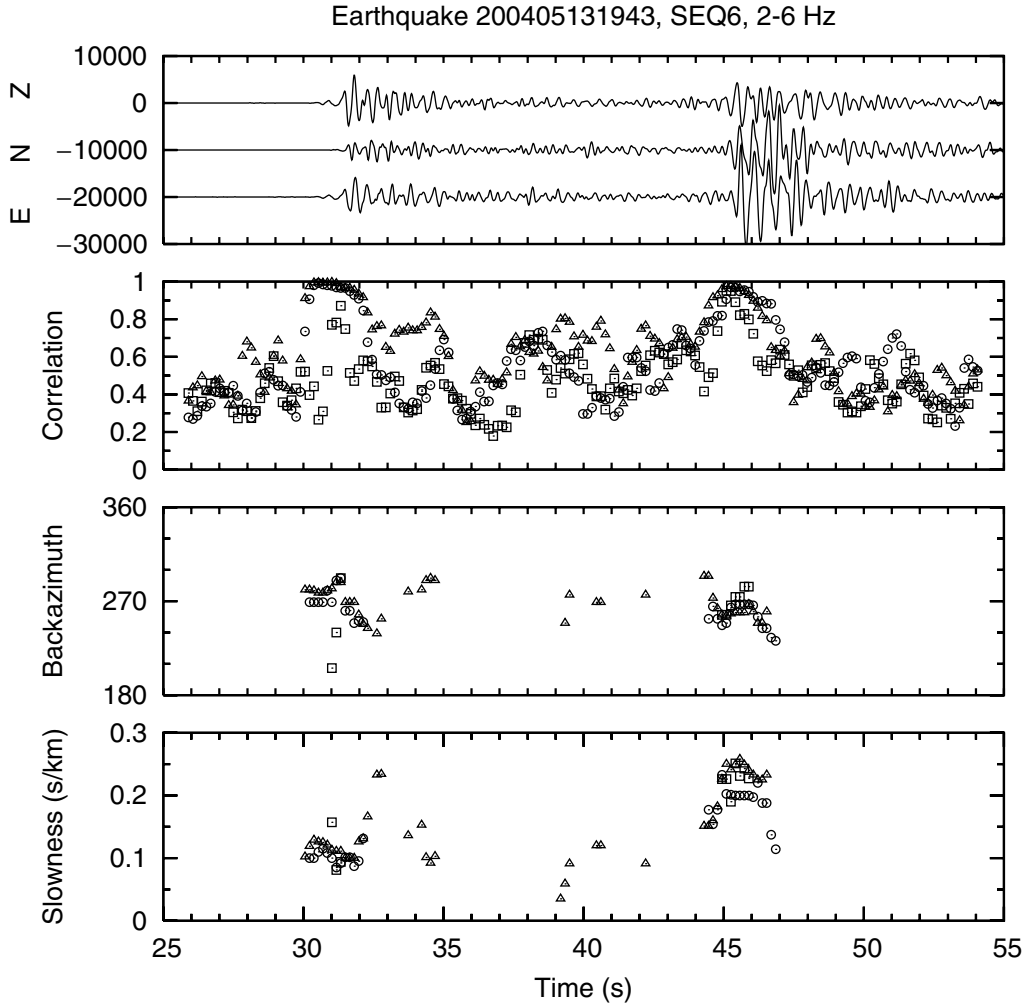


**Figure 5.** Results of the ZLCC analysis of earthquake 200405131943 at the Sequim array. The three components recorded at station SEQ6 are shown after filtering, in the top panel. The back-azimuth and slowness values are shown only for windows with correlations greater than 0.75. The results from the analysis of the vertical, north–south, and east–west components are shown by triangles, squares, and circles, respectively. Note that for this earthquake, the radial direction is east–west.

on, 1976) for local earthquakes and the Herrin velocity model (Herrin, 1968) for regional events. Assuming that $\Delta S_X = \Delta S_Y = \Delta S$, we computed $\Delta S$ as the difference between the slowness value obtained by the array analysis and the expected slowness. The back-azimuth difference $\Delta\varphi$ is computed from the difference between the array-determined back azimuth and the expected back azimuth.

The back-azimuth differences, $\Delta\varphi$, are plotted in Figure 6 for both the *P* waves and the *S* waves. In the lower panels of Figure 6, the stacking of the distributions for the *P* waves and the *S* waves and the best-fit Gaussian function are shown. The slowness differences, $\Delta S$, for the *P* waves and the *S* waves at each array and the stacks over the three arrays are plotted in Figure 7. Figure 8 shows the distributions of slowness obtained by array analysis for the *P* waves and the *S* waves at each array and their stacking. No evident relations between slowness and back-azimuth differences and the back azimuth were seen, although the azimuth distribution of the earthquakes is strongly nonuniform.

Because the three arrays showed comparable responses, we assume that they sample similar statistical variables. Stacked distributions of back-azimuth and slowness differences resemble normal distributions, as expected. The best-fit Gaussian functions for these distributions give the mean values and standard deviations of $\Delta\varphi_P \pm \sigma_{\Delta\varphi P} = 1.8° \pm 10.1°$, $\Delta\varphi_S \pm \sigma_{\Delta\varphi S} = -1.4° \pm 7.8°$ for the back-azimuth differences, and $\Delta S_P \pm \sigma_{\Delta SP} = -0.011 \pm 0.021$ sec/km and $\Delta S_S \pm \sigma_{\Delta SS} = -0.017 \pm 0.033$ sec/km for the two slowness distributions, where subscripts *P* and *S* stand for the *P* waves and the *S* waves, respectively. The mean values of $\Delta\varphi_P$ and $\Delta\varphi_S$ are much smaller than the corresponding standard deviations, and therefore they are negligible. The mean values of $\Delta S_P$ and $\Delta S_S$ are negative and have magnitudes comparable to those of the standard deviations, indicating that the array estimates of slowness are slightly smaller than the expected values. The bias for the *S* waves can be explained by the presence of *SV*-to-*P* converted energy in the same window containing the *S* direct phase, which increases the apparent velocity. The value of $\Delta S_P$ ($-0.011$ sec/km) is intriguing and more difficult to explain. A possible explanation might be that the velocity models used to compute the theoretical slowness do not take into account a possible horizontal velocity gradient.

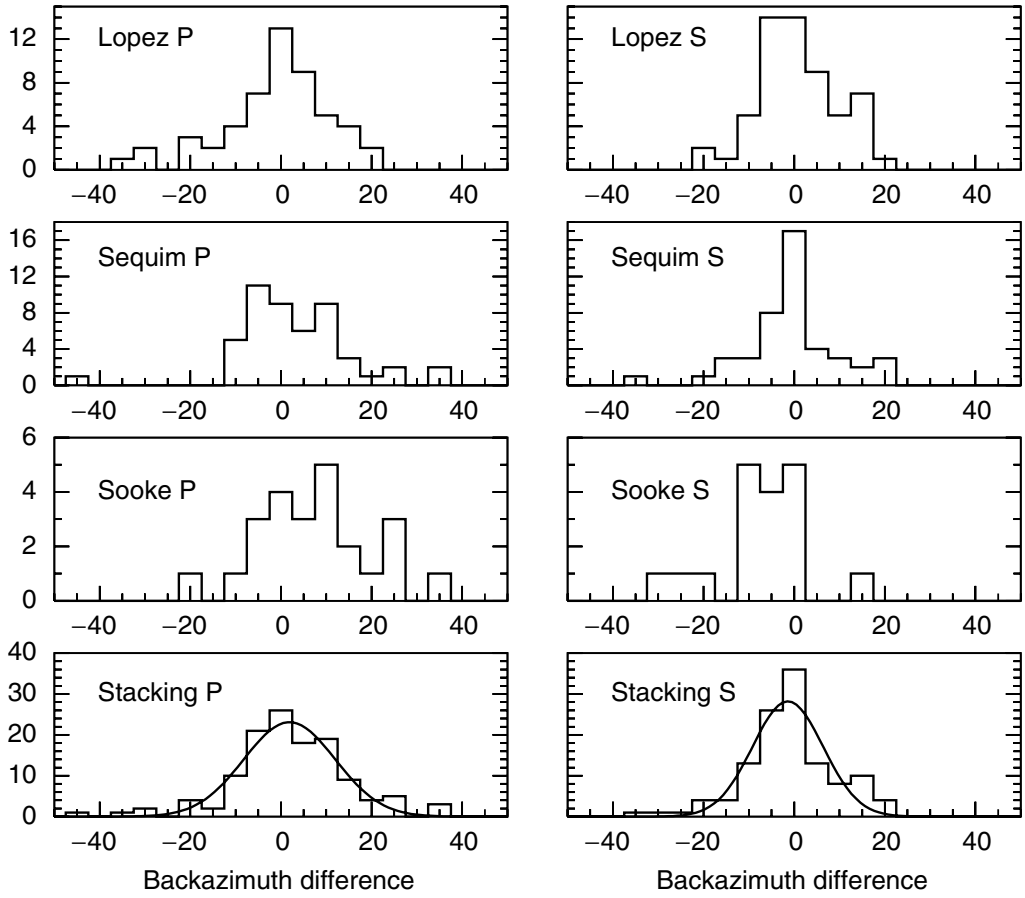


**Figure 6.** Distribution of back-azimuth differences between results obtained by array analysis and network determined locations. The data were computed for the three arrays for *P* waves (left column) and *S* waves (right column). The bottom panels show the stacking of the three-array distributions and the best-fit Gaussian function.

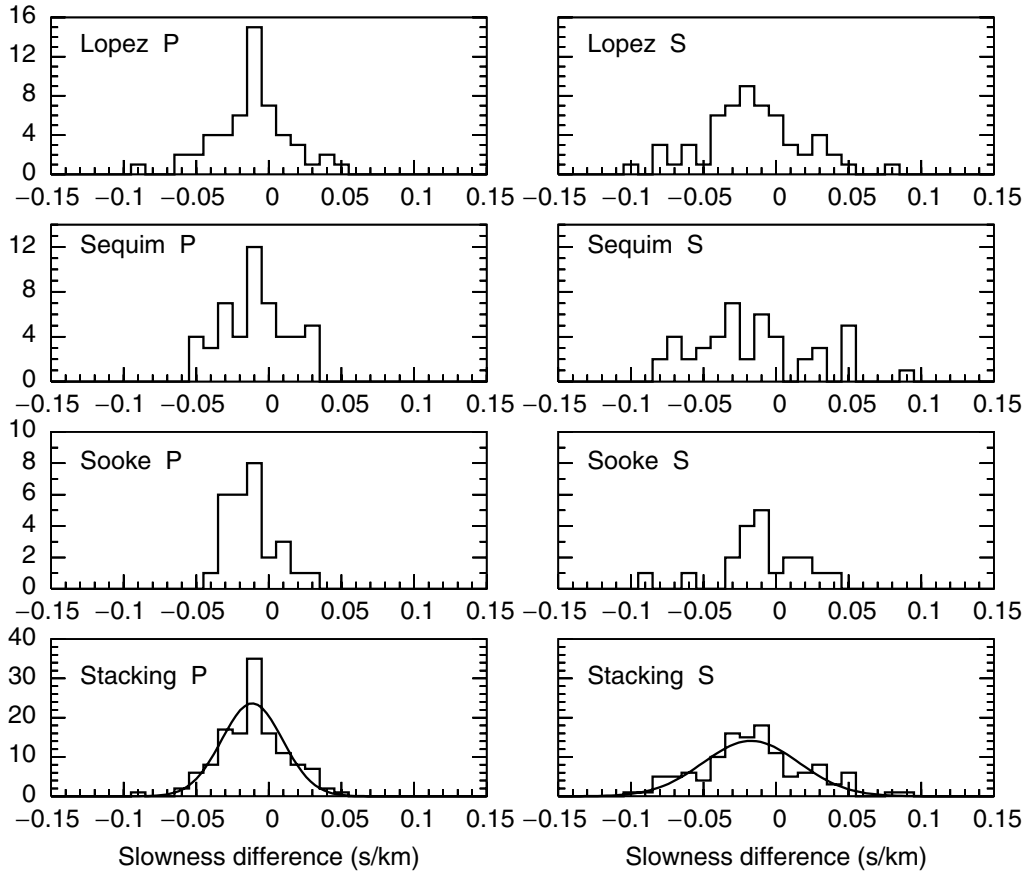


**Figure 7.** Distribution of slowness differences between results obtained by array analysis and network determined locations, as in Figure 6, for slowness.

The mean values of the stacked distributions of slowness and their standard deviations are $S_P \pm \sigma_{SP} = 0.128 \pm 0.021$ sec/km and $S_S \pm \sigma_{SS} = 0.224 \pm 0.031$ sec/km for the *P* waves and the *S* waves, respectively (Fig. 8). It is of note that the ratio $S_S/S_P$ is 1.75, while the standard deviations are practically identical to those computed for the slowness difference distributions.

An important result of this analysis is that the *P*-wave results have a standard deviation ($\sigma_{SP} = 0.021$ sec/km) significantly smaller than the *S*-wave standard deviation ($\sigma_{SS} = 0.033$ sec/km). In contrast, the standard deviation of the *P*-wave back azimuth ($\sigma_{\Delta\varphi P} = 10.1°$) is greater than the corresponding *S*-wave standard deviation ($\sigma_{\Delta\varphi S} = 7.8°$). The results for the *P* waves have smaller errors in terms of the slowness because they have a higher signal-to-noise ratio and the contamination from converted waves is usually negligible. However, the error in the back azimuth can be large due to the very low slowness value. In contrast, the results of the *S*-wave analysis show a larger slowness error than expected due to the generally lower signal-to-noise ratio and to the presence of *SV*-to-*P* converted energy and scattered energy, although they show a smaller error for the back azimuth, which is a direct consequence of the greater slowness value.

The difference between the array-determined and expected values for the propagation parameters of the seismic signal is easily computed for back azimuth and slowness separately. However, a more diagnostic parameter is a measure of the difference between the observed and expected wavefronts. This can be computed from the scalar product of the two unit vectors normal to the wavefronts. From the array analysis, we estimated the 2D slowness vector in the horizontal plane $\mathbf{S} = (S_X, S_Y)$. The vertical component $S_Z$ of the slowness vector is given by

$$S_Z = \frac{S}{\tan(\alpha)} = \frac{\sqrt{1 - V_E^2 S^2}}{V_E}, \tag{6}$$

where the incidence angle $\alpha$ (measured from the vertical) is given by

$$\alpha = \arcsin(V_E S), \tag{7}$$

in which $V_E$ is the effective wave velocity in the uppermost layer ($V_E \leq V = 1/S$), and $S$ is the modulus of the horizontal slowness vector. Using equation (6), we computed the array-determined and the expected slowness vectors in three dimensions. Once they were normalized, the inverse cosine of their scalar product gave the angle $\xi$ between the two wavefronts. The effective velocity $V_E$ in the upper layer was estimated through equation (7) using the angle $\alpha$ ob-

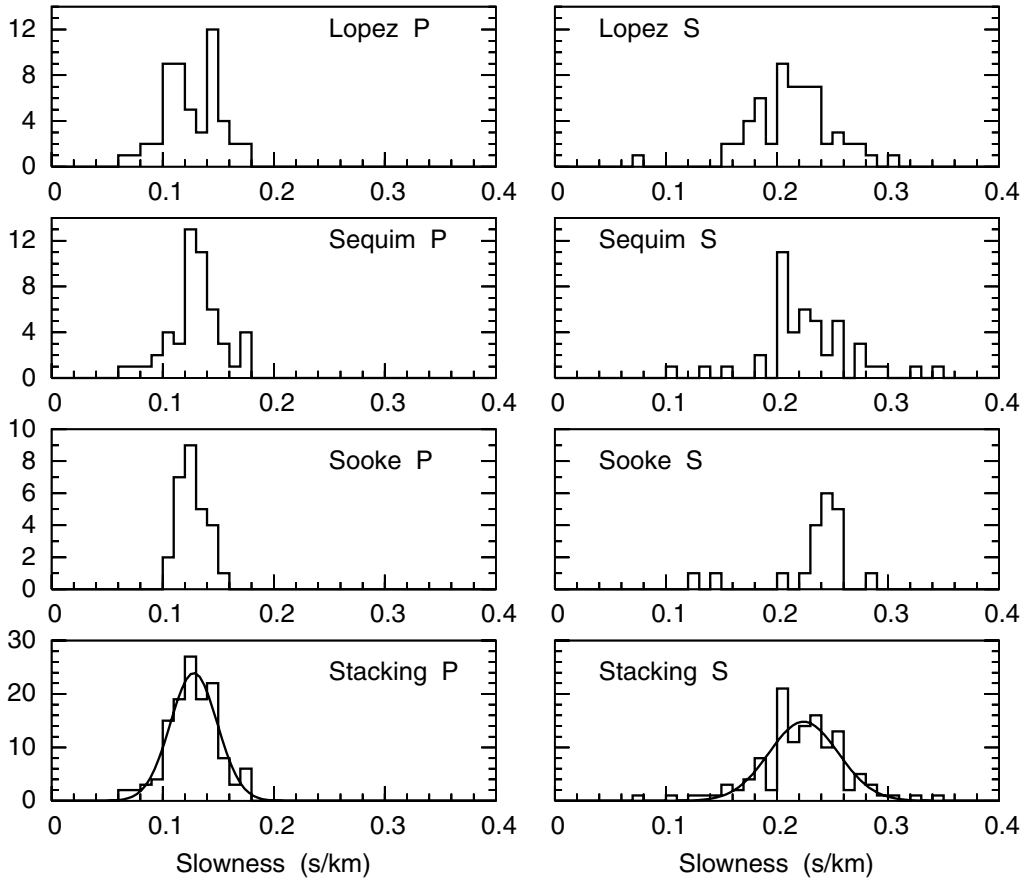


**Figure 8.** Distribution of the slowness values estimated by the array analysis at the three arrays for *P* waves (left column) and *S* waves (right column). The stacking over the three arrays and their fit with a Gaussian function are depicted in the bottom panels.

tained by the polarization analysis of several *P* waves. This procedure yielded values close to $V_P = 4.5$ km/sec (and hence $V_S = 2.57$ km/sec) for all three arrays. We have estimated the angle $\xi$ for both the *P* waves and the *S* waves at the three arrays using these values of $V_P$ and $V_S$ for the near surface *P*-wave and *S*-wave velocities, respectively. The two stacked distributions shown in Figure 9 are very similar with the maxima at 6°–8° and 4°–6° for the *P* waves and the *S* waves, respectively. The angle $\xi$ gives a rough idea of the error in the source location produced by the error in the estimate of the propagation parameters. In the simplest case of a half-space velocity model, the distance between the true and observed sources would be on the order of $D\sin(\xi)$, where *D* is the hypocenter distance. In the more realistic case of a vertical velocity gradient, the ray-path bending further increases the distance between the apparent and real sources.

## Probabilistic Source Location

To compare how the error estimates for the slowness vector from array analysis propagate back into the source locations, we used a source location procedure based on the evaluation of a probability density function (PDF) over a 3D grid given a velocity model and the estimation of the slowness vector components from earthquake the *P* waves and the *S* waves recorded at two or more arrays. The probability that the source is located at $(x, y, z)$, given the slowness vector $\mathbf{S}^0$ estimated at the array *a*, is

$$P_a(x, y, z) = \exp\{-0.5[\mathbf{S}^T - \mathbf{S}^0]^T[\mathrm{Cov}(S)]^{-1}[\mathbf{S}^T - \mathbf{S}^0]\}, \tag{8}$$

where $\mathbf{S}^T$ is the expected slowness vector corresponding to the position $(x, y, z)$, given a velocity model. $\mathrm{Cov}(S)$ is defined as

$$\mathrm{Cov}(S) = \sigma_S^2\mathbf{I}, \tag{9}$$

where $\mathbf{I}$ is the $2 \times 2$ unit matrix (Saccorotti and Del Pezzo, 2000; La Rocca *et al.*, 2004). If an estimation $t^0$ of the travel time is also available, as in the case of earthquakes, we can improve the estimation of the source position probability as follows:

$$P_a(x, y, z) = \exp\{-0.5[\mathbf{S}^T - \mathbf{S}^0]^T[\mathrm{Cov}(S)]^{-1}[\mathbf{S}^T - \mathbf{S}^0]\} \times \exp[-0.5(t^T - t^0)^2/\sigma_t^2]. \tag{10}$$

When more independent estimates of the slowness vector at different arrays are available, the overall probability function

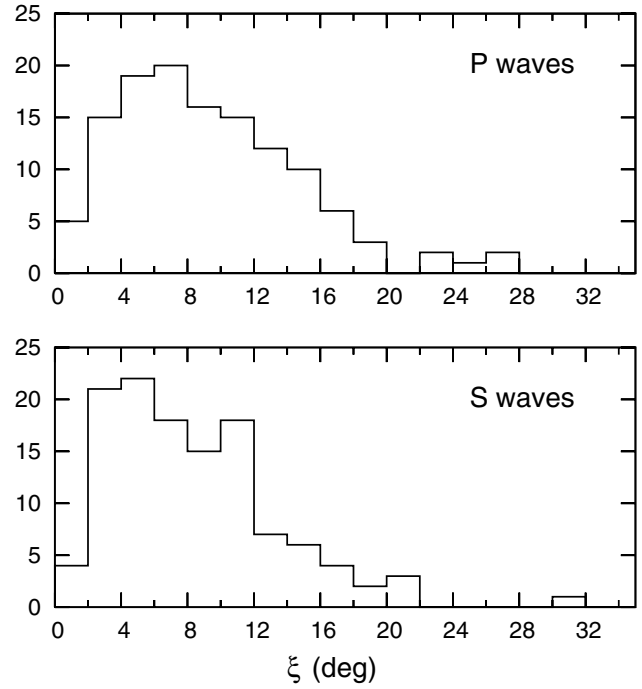


**Figure 9.** Distribution of the angle $\xi$ computed for the *P* waves and *S* waves. The results from the three arrays have been stacked.

is given by the product of each array PDF. In our case,

$$P(x, y, z) = P_{\mathrm{LOP}}(x, y, z)P_{\mathrm{SEQ}}(x, y, z)P_{\mathrm{SOK}}(x, y, z). \quad (11)$$

In the same way, at one array the probability that a *P*-*S*-wave pair shares the same spatial and temporal location (i.e., that they are radiated by the same source), is given by

$$P(x, y, z) = P_P(x, y, z)P_S(x, y, z). \quad (12)$$

This location method is very flexible because all of the information available about the slowness components and travel time of the seismic signals can be considered individually or all together. The minimum number of parameters needed for a location is the slowness vector for a single phase and its travel time at one of the arrays. If the travel time is not known, the minimum number of parameters is the slowness vector at two arrays. If there are data from several arrays (equation 11) for more than one phase (equation 12) and travel-time information, a more robust source location can be obtained. The location of one phase from only one array (equation 10) gives a unique solution with a maximum of the PDF near 1 (because the PDF is normalized by integrating over the entire volume spanned by the search grid). On the other hand, when using more than a single estimated slowness (using two different phases at the same array or using slownesses from two or more arrays) the solution may have a PDF much less than 1 and may not exist at all. In cases where various estimates of slowness and travel times are not compatible with the same source, the PDF maximum is very small. In these cases, we consider the PDF not normalizable, and no solutions are found by the probabilistic source location. The location using data from only one array is not possible for tremors because the travel time is unknown. For events in which the travel time is known, the probabilistic location using only one array can be considered less reliable than in the case of multiple arrays. Indeed, using only one array, the error for the estimated wavefront is propagated back into the location without the possibility of compensation from other estimates.

We used several combinations of data types to test the location procedures for the earthquakes. Figure 10 shows the results of several tests conducted with the evaluation of the PDF given by equation (8) at each array, using the expected slowness values of the *S* waves corresponding to the chosen source position. Then the three PDFs (one for each array) are multiplied to obtain the final location (equation 11). A range of depths and distances were tested to see how the PDF changes. As expected, the best results were obtained for sources near to or inside the array area. Even when well located, more distant sources are characterized by a rapid broadening of the PDF function as the distance increases. Bearing in mind these considerations, we located all of the local earthquakes recorded by at least two arrays using the *S*-wave slowness without considering travel times. Table 1 contains the details of the local earthquakes used, including the network-determined hypocenter data (depth and distance from each array) and the differences in slowness, back azimuth, and $\xi$ angle estimated at each array. The horizontal and vertical differences, $\Delta H$ and $\Delta Z$, between the maximum of the PDF and the catalog hypocenter are also shown.

Figure 11 shows the results of five examples of the earthquake locations obtained using only the slowness of the *S* phase. The events 06201910, 06240757, and 07081913 were recorded by all of the arrays, while the other two were recorded by only two arrays. The results of the probabilistic source location for most of the nearby earthquakes, 04050129, 05100345, 06060031, 06201910, 07110955, 07140044, and 07160345, are good, with $\Delta H \leq 10$ km and $\Delta Z < 5$ km, even though several of them were located using data from only two arrays. However, in many cases, the quality of the array analysis is not very good, as indicated by the angle $\xi$, which is sometimes greater than 10°. Some nearby earthquakes were characterized by poor array results, such as 06240757 ($\xi = 17.6°$ at Lopez), 07081913 ($\xi = 9.1°$ at Sequim), and 07180856 ($\xi = 8.0°$ at Lopez and $\xi = 11.5°$ at Sequim). Even in these cases, the probabilistic source locations are not grossly different from the catalog values.

Many of the earthquakes analyzed were located quite far from the array sites, with epicenter distances of up to 176 km (event 07031931). However, for the events with array parameters close to the expected values, and for those in which the deviations compensated for each other at the different arrays (06271140, 06280358, 07031931, 07051148,

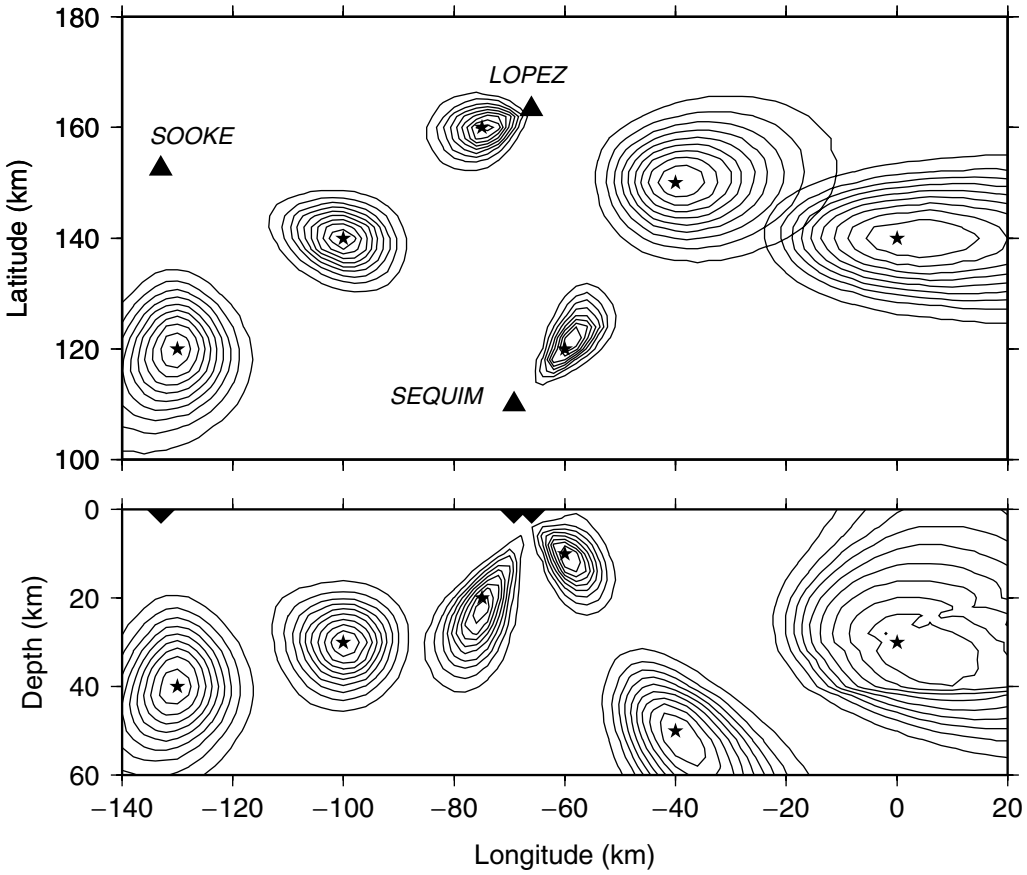


**Figure 10.** Examples of probabilistic source location using the slowness values corresponding to the grid nodes (indicated by stars). Contours depict the probability that the source is located inside the bounded volume, from 0.1 (innermost contour) to 0.9 (outermost contour). All three arrays were used here, using $\sigma_S = 0.033$ sec /km in equation (9), as found by the analysis of the *S* waves. As expected, the results are better for sources inside the array triangle or very close around it. Farther sources, even if well located, are characterized by a rapid broadening of the PDF function as the distance increases.

07180805, 07190432), the probabilistic source locations give acceptable results ($\Delta H < 25$ km and $\Delta Z < 20$ km).

All of the earthquakes reported in Table 1 were also located using the slowness estimates for the *P* wave, with results comparable to those discussed in this section and summarized in Table 1 for the *S* wave. The probabilistic source location was also computed taking into account the estimated travel times, which obtained results much closer to the network locations. However, this kind of source location is not relevant for the deep tremor array experiment, in which phase timing is not possible, and therefore we do not discuss those results here.

## Analysis of Deep Tremor

Deep tremor in the Puget Sound area occurs almost periodically (every $14 \pm 2$ months) and is associated with slow-slip events that are located along the Cascadia subduction zone (Dragert *et al.*, 2002; Rogers and Dragert, 2003). The complexity of this seismic signal, which is characterized by an emergent onset, the absence of impulsive phases, the dominance of *S*-wave energy, migration of the source with time, and a wide depth range (10–80 km), has been noted in several studies that have analyzed seismic network data (McCausland *et al.*, 2005; Kao *et al.*, 2006; Kao *et al.*, 2007).

The main aim of this three-array study was the recording of the ETS episodes that occurred during the summer of 2004. The whole tremor sequence was detected at the arrays for more than 20 days, starting on 6 July. Strong signals located in the North Puget Sound area lasted more than a week. One of the primary purposes of this array study was to determine reliable locations for tremor sources. We applied array analysis and the probabilistic location technique described in this article to several tremor periods. As expected, the best results were obtained for tremor sources where the epicenters were located inside the array triangle and when only one source was active at a time or many sources were clustered in a small volume.

Figure 12 shows the results for the array analysis for 10 min of strong tremor. For each array, one transverse component seismogram is shown, along with the back azimuth and slowness of windows with correlations higher than a suitable threshold (0.9 at Lopez and 0.8 at Sequim and Sooke).

Table 1

Differences between Array Analysis and Network-Determined Propagation Parameters and Source Location

| | | Lopez | | | | Sequim | | | | Sooke | | | | | |
|---|---|---|---|---|---|---|---|---|---|---|---|---|---|---|---|
| Event | Depth (km) | Distance (km) | $\Delta S$ (sec/km) | $\Delta\varphi$ (deg) | $\xi$ (deg) | Distance (km) | $\Delta S$ (sec/km) | $\Delta\varphi$ (deg) | $\xi$ (deg) | Distance (km) | $\Delta S$ (sec/km) | $\Delta\varphi$ (deg) | $\xi$ (deg) | $\Delta H$ (km) | $\Delta Z$ (km) |
| 200404050129 | 25.71 | 87 | 0.026 | −3 | 5.6 | 45 | −0.009 | −5 | 3.3 | 122 | — | — | — | 4.7 | −1.7 |
| 200404251442 | 17.70 | 106 | −0.02275 | 15 | 10.5 | 82 | −0.00475 | −3 | 2.2 | 157 | — | — | — | 38.0 | 0.3 |
| 200404292345 | 21.69 | 132 | −0.02325 | 1 | 4.1 | 90 | 0.02075 | 1 | 4.3 | 167 | — | — | — | 37.3 | −7.7 |
| 200405100345 | 21.55 | 37 | −0.01575 | 2 | 3.1 | 25 | 0.04525 | −8 | 9.5 | 83 | — | — | — | 5.6 | −4.5 |
| 200405131943 | 0.03 | 118 | 0.01775 | −1 | 3.2 | 98 | −0.0695 | 0 | 12.9 | 61 | — | — | — | 2.8 | 64.0 |
| 200405150130 | 0.02 | 117 | 0.02275 | 5 | 5.0 | 97 | −0.0255 | −4 | 5.7 | 61 | — | — | — | 19.9 | 38.0 |
| 200405151033 | 0.04 | 117 | −0.07875 | −2 | 14.5 | 97 | −0.0475 | 0 | 9.0 | 61 | — | — | — | 9.5 | 56 |
| 200406060031 | 26.58 | 32 | −0.03025 | −1 | 3.5 | 26 | 0.01725 | 22 | 11.6 | 79 | — | — | — | 9.9 | −0.6 |
| 200406111140 | 24.70 | 136 | −0.0385 | 6 | 6.7 | 87 | 0.0225 | −15 | 11.2 | 160 | — | — | — | 59.9 | −16.7 |
| 200406181019 | 6.97 | 95 | — | — | — | 92 | −0.01775 | −1 | 3.6 | 157 | −0.01475 | −2 | 3.1 | 21.7 | 23.0 |
| 200406181038 | 7.36 | 96 | −0.01775 | −1 | 3.6 | 95 | −0.05975 | 1 | 11.2 | 158 | −0.02075 | −8 | 6.5 | 18.0 | 32.6 |
| 200406201910 | 23.31 | 36 | 0.039 | 9 | 9.3 | 68 | −0.06825 | 22 | 17.1 | 35 | −0.02225 | −4 | 4.5 | 7.6 | 2.1 |
| 200406240757 | 19.89 | 23 | 0.0795 | 14 | 17.6 | 67 | −0.02425 | 0 | 4.6 | 91 | −0.014 | −11 | 7.6 | 6.0 | −14.9 |
| 200406271140 | 0.02 | 48 | −0.03175 | 10 | 9.4 | 70 | −0.04175 | −14 | 12.2 | 115 | −0.02775 | −3 | 5.7 | 20.5 | 16.0 |
| 200406280358 | 1.47 | 49 | −0.017 | 15 | 11.0 | 70 | 0.04825 | −17 | 17.2 | 116 | −0.036 | 0 | 6.9 | 25.0 | 4.5 |
| 200407031931 | 13.12 | 130 | −0.03875 | 2 | 7.4 | 99 | −0.0495 | 6 | 9.9 | 176 | 0.03475 | 1 | 6.4 | 20.9 | 20.9 |
| 200407051148 | 10.57 | 80 | 0.00225 | 8 | 5.5 | 85 | −0.02975 | 11 | 9.2 | 144 | −0.03275 | 13 | 10.2 | 17.5 | 13.4 |
| 200407081913 | 27.44 | 61 | −0.0145 | −11 | 7.1 | 8 | 0.0295 | −36 | 9.1 | 84 | −0.01025 | −8 | 5.4 | 13.8 | 12.6 |
| 200407101635 | 15.90 | 99 | −0.0805 | 1 | 14.6 | 81 | −0.0405 | −9 | 9.3 | 154 | — | — | — | 20.3 | 34.1 |
| 200407110955 | 17.78 | 28 | −0.023 | −8 | 6.1 | 41 | 0.0015 | −2 | 1.3 | 87 | −0.01775 | 1 | 3.5 | 4.0 | 2.2 |
| 200407140044 | 22.37 | 18 | −0.0025 | 0 | 0.4 | 54 | 0.0455 | 5 | 10.0 | 85 | −0.00725 | −11 | 7.3 | 1.4 | −1.4 |
| 200407160345 | 23.96 | 12 | −0.17925 | −22 | 30.9 | 50 | — | — | — | 57 | 0.00325 | −18 | 11.5 | 10.4 | 2.0 |
| 200407180805 | 23.25 | 112 | −0.0225 | 1 | 4.3 | 66 | −0.00025 | 0 | 0.1 | 143 | — | — | — | 12.7 | 8.7 |
| 200407180856 | 15.01 | 42 | −0.0385 | 6 | 8.0 | 94 | −0.0545 | 9 | 11.5 | 70 | −0.0125 | −4 | 3.6 | 14.3 | 25.0 |
| 200407190432 | 24.10 | 83 | −0.02675 | 0 | 5.0 | 55 | −0.037 | 0 | 6.7 | 130 | 0.0285 | −27 | 19.5 | 11.0 | 15.9 |

The local earthquakes recorded by at least two arrays located using the probabilistic method applied only to the *S* waves. The events are named by date and time. For each array, the epicenter distance, the slowness difference $\Delta S$ (estimated minus expected), the back-azimuth difference $\Delta\varphi$ (estimated minus expected), and $\xi$ angle are shown. The horizontal and vertical differences ($\Delta H$ and $\Delta Z$) between the hypocenters estimated by the probabilistic method and the network locations are also shown.

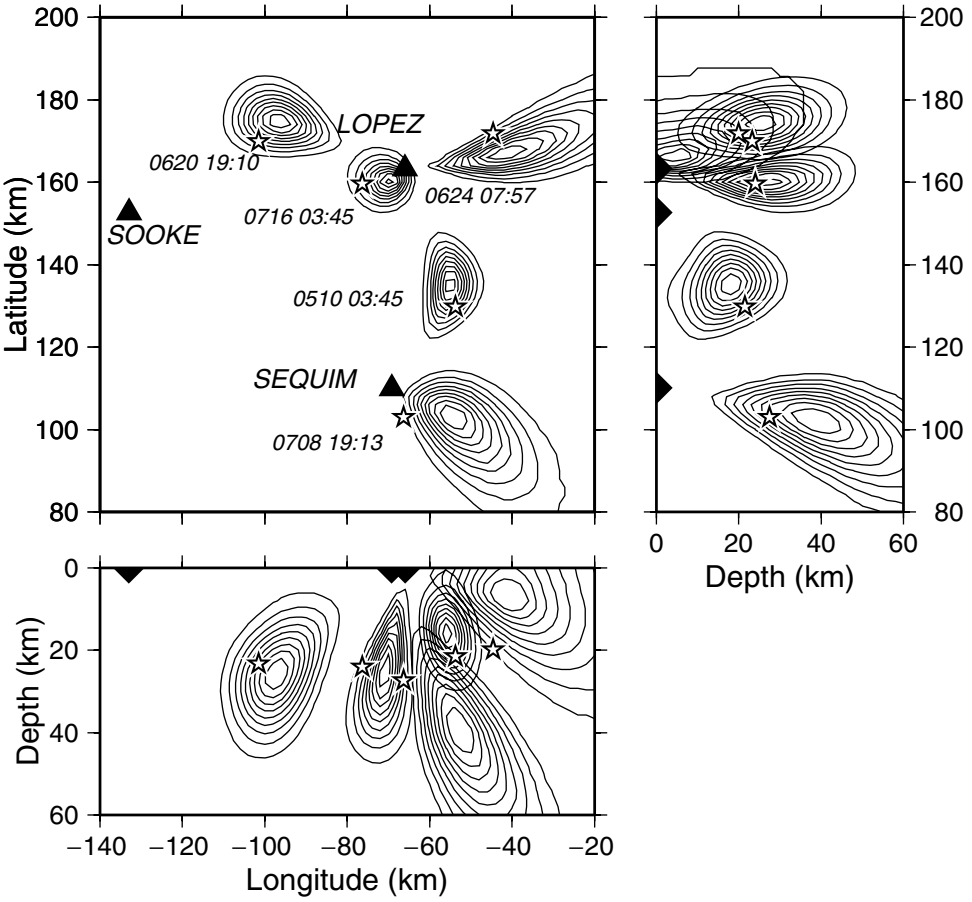


**Figure 11.** Probabilistic source location of five local earthquakes. The stars represent the hypocenters located using the PNSN data, while the contour lines represent the normalized probability computed using only the estimated slowness of the *S* wave. Two of these events, 200405100345 and 200407160345, were recorded by only two arrays. Details of these and more located earthquakes are summarized in Table 1.

For this tremor, the slowness at the three arrays was stable over time, and the three back azimuths point to the same epicenter near the middle of the array area. These characteristics of the tremor signal were often seen at the beginning of the ETS event of July 2004 (McCausland, 2006). At the Sequim array, the slowness and the back-azimuth values both had a larger spread than for the other two arrays. This spread was a consequence of the general lower quality of the signals recorded at this site. Indeed, the background seismic noise at the Sequim array had amplitudes at least twice that of Lopez and about three to four times the average noise recorded at Sooke. The coherence of the seismic noise at the Sequim array was often higher than at the other two arrays, and site responses at the seven stations of this array appeared to be more heterogeneous than at the Lopez and Sooke arrays, probably due to variable local geology.

The average values of slowness were 0.202 sec/km at the Lopez array, 0.254 sec/km at Sequim, and 0.195 sec/km at Sooke, while the mean back-azimuth values were 232°, 322°, and 107°, respectively. These values were associated with the *S*-wave slowness uncertainty $\sigma_S = 0.033$ sec/km and were used to compute the probabilistic source location, the PDF, which is shown in Figure 13. Many hours of tremor have been located using this method, with reliable results in all cases of one active source located inside the array area. The maxima of the location PDFs for many tremor bursts recorded on 9, 11, and 15 July are also shown in Figure 13. Unfortunately, the analysis of the tremor signals very often indicated clearly the presence of more than one source active at the same time, but located significantly far from each other. Although not described here because it is beyond the scope of the present study, detailed analysis of the PNSN network data for an extended period of time gave results that were in good agreement with our probabilistic source location (McCausland, 2006).

## Discussion and Conclusions

The availability of several tens of local and regional earthquakes that were well located by a regional network and recorded by three small-aperture arrays provides an interesting opportunity to test the reliability of seismic array analysis methods. We applied the ZLCC method to 51 earthquakes and compared the estimated slowness and back azi-

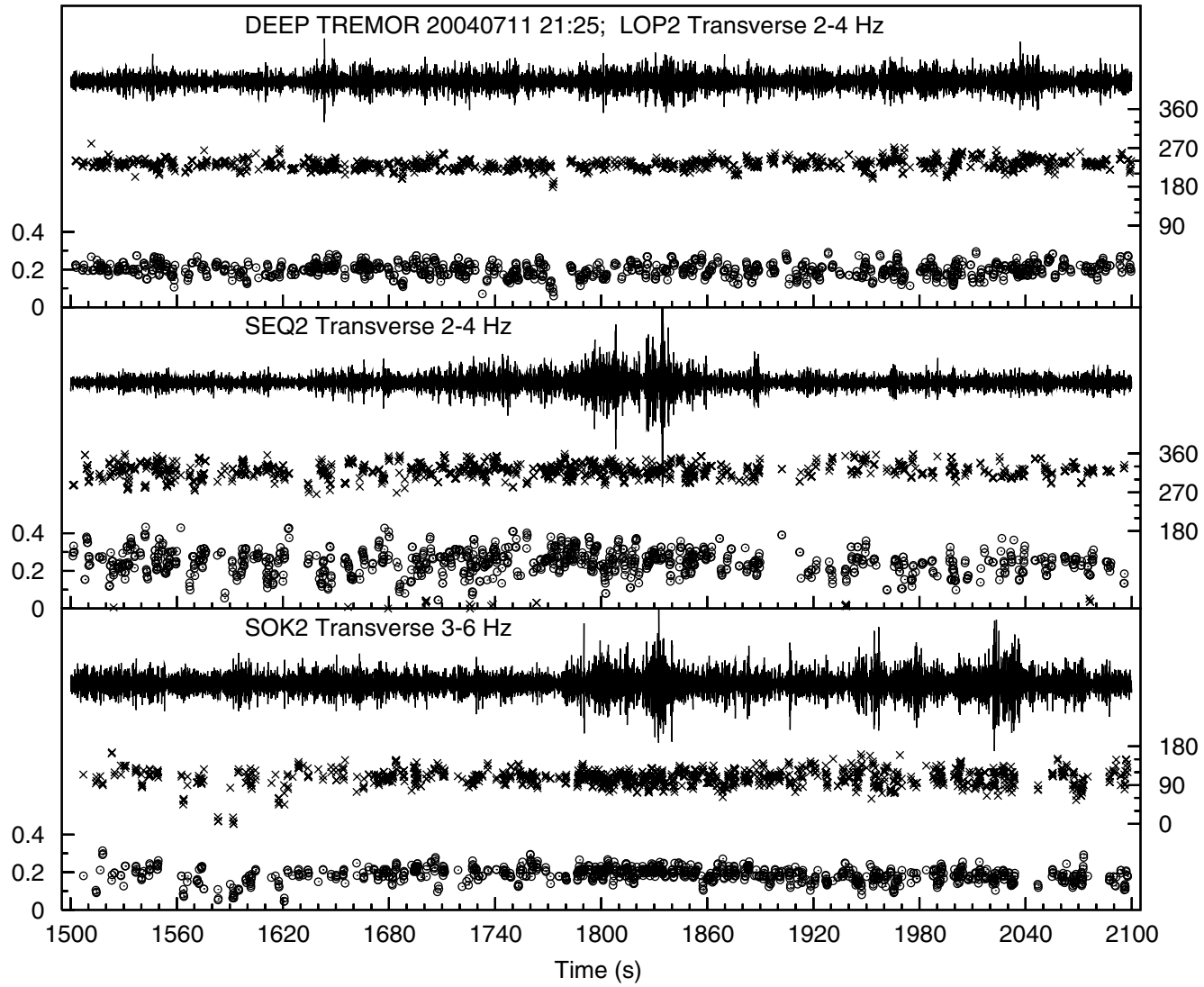


**Figure 12.** Results of ZLCC analysis for ten minutes of deep tremor recorded at the three arrays on 11 July 2004 at 21:25. Each plot shows one transverse-component-filtered seismogram, the back azimuth (crosses, right scale), and slowness (circles, left scale) of the windows where the correlation exceeds the threshold of 0.9 at the Lopez array and 0.8 at the Sequim and Sooke arrays.

muth with the expected values, to quantify the uncertainty in the estimates of these parameters. From the distributions of slowness and back-azimuth differences computed for both the *P* waves and the *S* waves, we estimated the uncertainty of the slowness vector components, or in other words, the array resolution capability. This estimation allowed for a quantification of the correlation range around the maximum of the correlation spectrum within which the true solution was found with a quantifiable probability.

These theoretical array responses and experimental results from the analysis of earthquakes confirm that a lot of care must be given to the array configuration when planning a field survey. Because the errors in the estimated propagation parameters increase exponentially as the slowness decreases, the analysis of high-velocity signals can produce unreliable results. High-velocity signals come from distant sources, such as teleseisms, as well as from very close sources where the direct waves reach the array with a small incidence angle. Therefore, the array size is a trade-off between site effects, which reduce the coherence of the wave field, and the array resolution capability, which increases with array aperture. The number of stations is a trade-off between the instrument and data management capability and the possibility of improving the quality of the results. Multichannel methods in the frequency domain usually give better and more stable results as the number of stations increases, even though the computing time rises rapidly.

Local earthquakes recorded at the three arrays provided a useful test for array-processing location methods. We applied a probabilistic source location procedure to tens of well-located local events to gain insight into the reliability of the method. The probabilistic source location method is

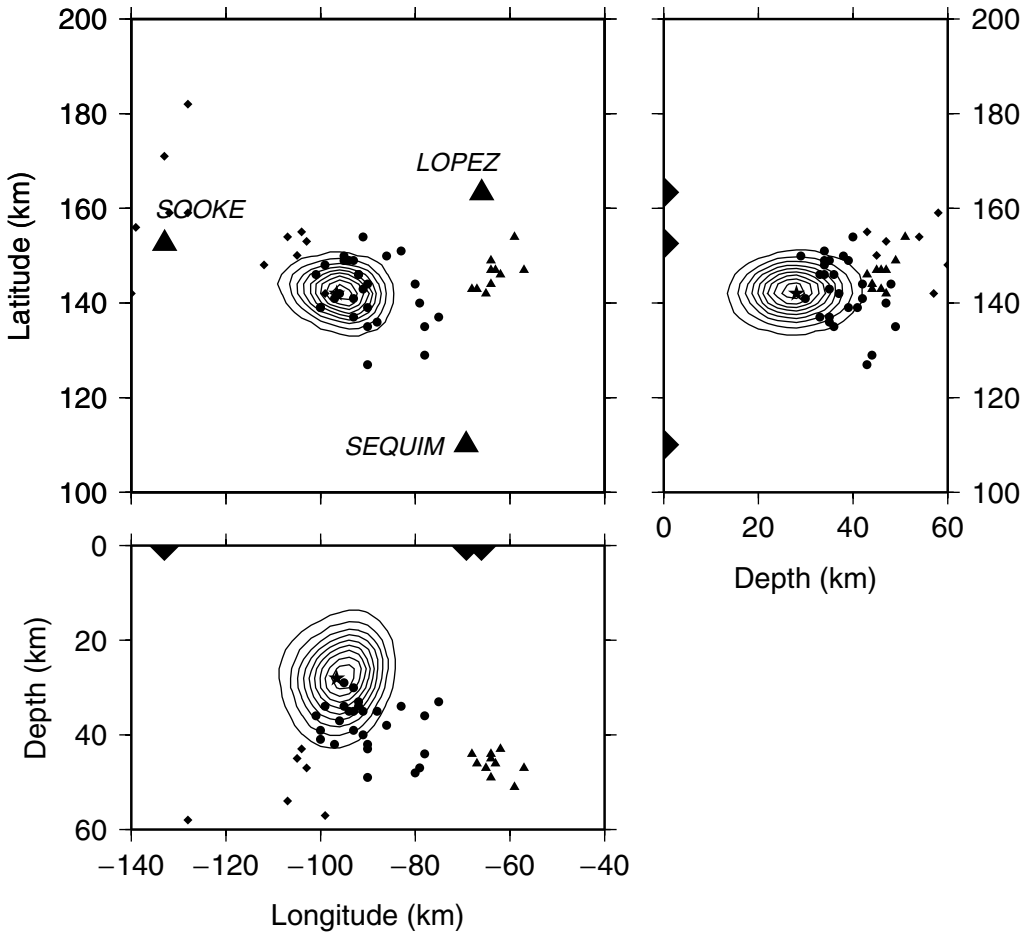


**Figure 13.** Probabilistic source location of several hours of deep tremor recorded on 9 July (triangles), 11 July (circles), and 15 July (diamonds). The contour lines show the PDF obtained by the location of the deep tremor shown in Figure 13. Only the slowness estimated by the array analysis of the transverse components at the three arrays was used for these locations.

appropriate for events, such as tremors, that do not have impulsive arrivals. For this kind of seismic signal, it is not possible to estimate the travel time. Therefore, as part of the test, we located earthquakes using only the slowness vector components of the *S* wave at two or three arrays to compare with the network locations. The results of these tests indicate that the solution is better for epicenters within or near the triangle bound by the arrays. Unfortunately, only one event occurred within this area during the study (Fig. 10), and several other events that were located close to the arrays were recorded by only one or two arrays. However, the results of the error analysis propagated onto the location space of the probabilistic location technique are consistent with the differences in estimated locations based on array analysis and the actual locations determined by conventional methods.

The probabilistic location of tremor sources allows for a reasonable estimate of the source depth in cases where tremor originates from only one place. The error associated with the hypocenter coordinates can be inferred from the PDF contours. For a source located near the middle of the array area and at a depth less than 40 km, the 70% probability volume has a horizontal radius of 8 km and a vertical radius of 10 km (Fig. 13). The error on the depth increases rapidly if the source is deeper than about 50 km. The method proved to be useful for the location of nonimpulsive signals, like deep tremors, giving reliable and stable results in the case of a single source or densely clustered sources (McCausland, 2006). The location of multiple-source deep tremors requires more complex and detailed analysis and is beyond the scope of this study.

## Acknowledgments

The array project in 2004 was funded by National Science Foundation project EAR-0337144. Some instruments used for the Lopez and Sequim arrays were financed and loaned by AMRA, Regione Campania, Italy. The Sooke array was provided by the Program for the Array Seismic Studies of the Continental Lithosphere (PASSCAL) instrument pool of the Incorporated Research Institutions for Seismology (IRIS). The authors are appreciative of the staff of the Pacific Geoscience Center for assistance with the Sooke array and for helpful discussions. Some of the figures were drawn using the GMT software by Wessel and Smith (1998). J. Pujol and two anonymous reviewers are gratefully acknowledged for their comments, which have greatly improved the quality of our manuscript.

## References

Capon, J. (1969). High resolution frequency-wave number spectrum analysis, *Proc. IEEE* **57,** 1408–1418.

Crosson, R. S. (1976). Crustal structure modeling of earthquake data 2: velocity structure of the Puget Sound region, Washington, *J. Geophys. Res.* **81,** 3047–3054.

Crotwell, H. P., T. Owens, and J. Ritsema (1999). The TauP toolkit: flexible seismic travel-time and ray-path utilities., *Seism. Res. Lett.* **70,** 154–160.

Del Pezzo, E., M. La Rocca, and J. Ibanez (1997). Observation of high frequency scattered waves using dense arrays at Teide volcano, *Bull. Seismol. Soc. Am.* **87,** 1637–1647.

Dragert, H., K. Wang, and T. S. James (2002). A silent slip event on the deeper Cascadia subduction interface, *Science* **292,** 1525–1528.

Frankel, A., S. Hough, P. Friberg, and R. Busby (1991). Observations of Loma Prieta aftershocks from a dense array in Sunnyvale, California, *Bull. Seismol. Soc. Am.* **81,** 1900–1922.

Goldstein, P., and R. J. Archuleta (1987). Array analysis of seismic signals, *Geophys. Res. Lett.* **14,** 13–16.

Goldstein, P., and R. J. Archuleta (1991). Deterministic frequency-wave number techniques and direct measurements of rupture propagation during earthquakes using a dense array: theory and methods, *J. Geophys. Res.* **97,** 6173–6185.

Herrin, E. (1968). 1968 Seismological tables for *P* phases, *Bull. Seismol. Soc. Am.* **58,** 1193–1241.

Kao, H., S.-J. Shan, H. Dragert, G. Rogers, J. F. Cassidy, K. Wang, T. S. James, and K. Ramachandran (2006). Spatial-temporal patterns of seismic tremors in northern Cascadia, *J. Geophys. Res.* **111,** B03309, doi 10.1029/2005JB003727.

Kao, H., S.-J. Shan, G. Rogers, and H. Dragert (2007). Migration characteristics of seismic tremors in the northern Cascadia margin, *Geophys. Res. Lett.* **34,** L03304, doi 10.1029/2006GL028430.

La Rocca, M., W. McCausland, D. Galluzzo, S. Malone, G. Saccorotti, and E. Del Pezzo (2005). Array measurements of deep tremor signals in the Cascadia subduction zone, *Geophys. Res. Lett.* **32,** L21319, doi 10.1029/2005GL023974.

La Rocca , M., G. Saccorotti, E. Del Pezzo, and J. Ibanez (2004). Probabilistic source location of explosion quakes at Stromboli volcano estimated with multiple array data, *J. Volcanol. Geotherm. Res.* **131,** 123–142.

McCausland, W. (2006). Tracking subduction tremor in Cascadia using regional network and small-aperture seismic array data, *Ph.D. Thesis*, University of Washington.

McCausland, W., S. Malone, and D. Johnson (2005). Temporal and spatial occurrence of deep non-volcanic tremor: from Washington to Northern California, *Geophys. Res. Lett.* **32,** L24311, doi 10.1029/2005GL024349.

Rogers, G., and H. Dragert (2003). Episodic tremor and slip on the Cascadia subduction zone: the chatter of silent slip, *Science* **300,** 1942–1943.

Saccorotti, G., and E. Del Pezzo (2000). A probabilistic approach to the inversion of data from a seismic array and its application to volcanic signals, *Geophys. J. Int.* **143,** 249–261.

Schmidt, R. O. (1986). Multiple emitter location and signal parameter estimation, *IEEE Trans. Antennas Propag.* **34,** 276–280.

Wessel, P., and W. H. F. Smith (1998). New, improved version of Generic Mapping Tools released, *EOS* **79,** 579.

Istituto Nazionale di Geofisica e Vulcanologia
Osservatorio Vesuviano
Via Diocleziano, 328
80124 Napoli, Italy
mlarocca@ov.ingv.it
galluzzo@ov.ingv.it
delpezzo@ov.ingv.it
(M.L.R., D.G., G.S., E.D.P.)

Department of Earth and Space Sciences
University of Washington
Box 351310, Office: ATG-226
Seattle, Washington 98195
steve@ess.washington.edu
(S.M., W.M.)

Manuscript received 31 August 2006